Adsorption, 1, 233–252 (1995)

Adsorptive Separation by Thermal Parametric Pumping Part II: Experimental Study of the Purification of Aqueous Phenolic Solutions at Pilot Scale

LICÍNIO M. FERREIRA* AND ALÍRIO E. RODRIGUES
Lab. of Separation and Reaction Engineering, School of Engineering, University of Porto, 4099 Porto Codex, Portugal

Abstract. In this work scale-up concerns in adsorptive parametric pumping operation in recuperative mode are studied. An experimental study of the purification of wastewater containing 100 ppm of phenol using a polymeric adsorbent (Duolite ES861-Rohm and Haas, France) is reported. A completely automated pilot plant (column and ancillary equipment, product receivers, sampling, collector and analytical devices) is described. The plant is computer controlled enabling automatic data acquisition for temperature, pressure and flowrate.

Parameters related with adsorption equilibrium, mass transfer and heat transfer resistances were determined in order to obtain basic information to simulate the process behavior.

Continuous and semicontinuous top feed parametric pumping experiments were carried out in a bed with 0.09 m diameter and 1 m long which represents a scale-up by a factor of 60 relative to previous works. Optimal operating conditions yielding the maximum productivity of the bottom product (phenol concentration <1 ppm), were achieved experimentally with the following conditions: average cycle time = 4 h, ratio $\phi_B/\phi_T = 2$ ($\phi_B = 0.27$), reservoir volume $Q(\pi/\omega) = 32.5$ ℓ, average flowrate = 0.24 ℓ/min. Based on these conditions, after 12 cycles of operation, 105 ℓ of treated water is obtained. Those optimal operating conditions were suggested by simulation studies presented in Part I (Ferreira and Rodrigues, 1995) of this work.

Good agreement was obtained between experimental and simulated results using the complete model developed in Part I (Ferreira and Rodrigues, 1995).

Keywords: parametric pumping, purification, pilot plant, phenolic solutions

Introduction

Parametric pumping has been used by several authors for separation and purification purposes at the laboratory scale. At the industrial scale, the Sirotherm process (Bolto, 1975), which uses thermal regenerated resins, presents some features common to parametric pumping. Basic aspects about the process were first introduced by Wilhelm (1966). As a classical example we emphasize the work developed by Wilhelm et al. (1968). These authors removed toluene from *n*-haptane using silica gel as adsorbent in a batch direct mode parametric pump.

The same system was treated by Chen et al. (1972, 1973) operating in continuous and semicontinuous modes. Sweed and Gregory (1971) removed NaCl from water using ion retardation resin (BioRad AG 11-A8). The system phenol-water/Duolite ES-861 was studied by Costa et al. (1982), Almeida et al. (1982) and Ramalho et al. (1991). Using a small scale experimental set-up those authors showed that it is possible to obtain almost pure water (<10 ppb phenol) using either the direct or the recuperative mode of operation. The present paper reports experiments for the same system (phenol-water/Duolite ES861 (Rohm and Haas, France)), using a pilot scale parametric pump operated in recuperative mode. The column diameter is now six times larger than the one used previously; since the column length is 1.7 times longer the volume scales by a factor of 60. Simulation results presented in Part I (Ferreira and Rodrigues, 1995) have guided the choice of optimal conditions. In fact process performance increases when cycle time (t_c) increases and ϕ_B/ϕ_T ratio decreases. Thus from simulations one can guarantee that $C_{bp} \leq 1$ ppm if $t_c = 4$ h and $\phi_B/\phi_T = 2$ keeping in mind that reasonable productivity has to be achieved.

*Present address: Chemical Engineering Department, University of Coimbra, 3000 Coimbra, Portugal.

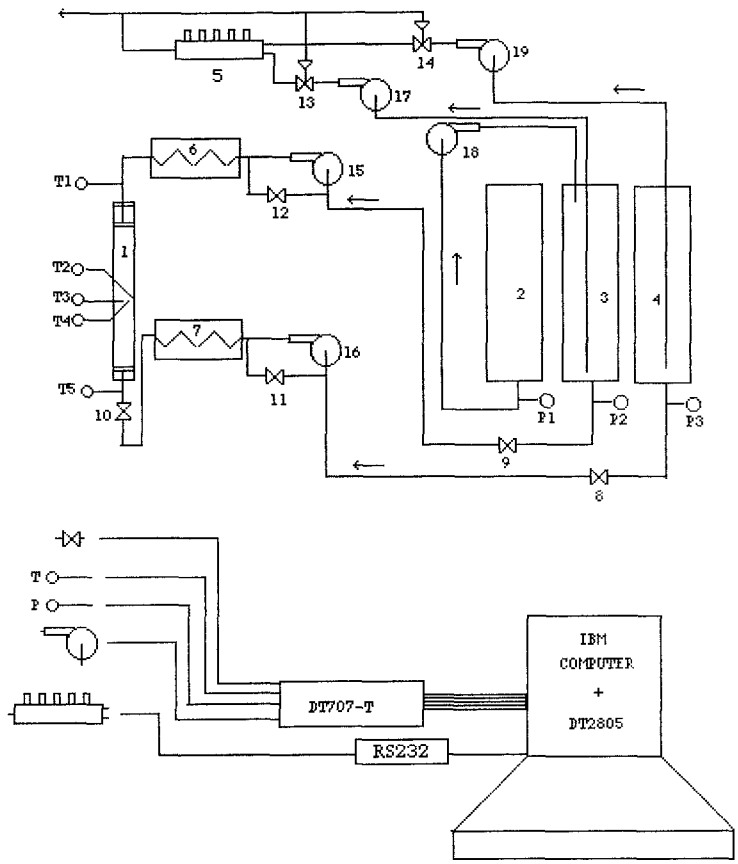

Fig. 1. Experimental set-up of the parametric pumping pilot plant. Legend: 1 Glass column G90-Amicon; 2 Feed reservoir; 3 Top reservoir; 4 Bottom reservoir; 5 Fraction collector—Gilson; 6–7 Heat exchangers; 8–12 two-ways solenoid valves; 13–14 three-ways solenoid valves; 15–16 Peristaltic pumps—Watson Marlow; 17–19 Peristaltic pumps—Gilson; T1–T5 Thermocouples (type K); P1–P3 Pressure transducers Schaevitz (type P510).

Table 1 summarizes the various experimental systems used in parametric pumping studies.

The work reported here was directed to the understanding of the scale-up concerns of parametric pumping and involves the following sections:

(i) the description and operation of a completely automated continuous recuperative parametric pumping unit, with feed to the top reservoir;
(ii) basic information related with adsorption equilibrium, mass transfer resistances and heat transfer in the fixed bed column;
(iii) simulation of the experimental parametric pumping runs.

Experimental Set-up

The experimental set-up of the completely automated pilot plant for recuperative parametric pumping is shown in Fig. 1. It can be divided in four sections: i) the column and the ancillary equipment, ii) the product receivers, iii) the sampling, collector and analytical devices and iv) the automation section.

Column and the Ancillary Equipment

The heart of the parametric pumping is a borosilicate packed column (Amicon G90 × 1000) with 0.09 m internal diameter and about 1 m height. The column consists of three subunits: the fixed assembly, the column unit and the adjuster assembly. The bed support is a 30 μm porosity polyethylene sinter. Five thermocouples (type K) are installed axially and radially in the column to measure the temperatures waves. The solution is passed through the column either downward (cold half cycle —20°C) or upward (hot half cycle —60°C) using the peristaltic pumps 15 or 16, respectively. During downward flow the solenoid valve 11 is open and the valve 12 is closed; the valves position is

Table 1. Summary of adsorbent and chemical systems used by thermal parametric pumping.

Adsorbent	Chemical system (liquid/solid adsorption or ion-exchange)	Reference
Activated carbon	Urea-water	Sweed (1971)
	Oxalic acid-water	Rice and Mackenzie (1973)
Silica gel	Toluene-*n*-heptane	Wilhelm et al. (1968)
		Pigford (1969)
		Chen et al. (1972, 1973, 1974)
	Toluene-*n*-heptane-aniline	Chen et al. (1974)
Ion retardation resin (BioRad AG11A8)	Sodium chloride-water	Sweed and Gregory (1971)
		Gregory and Sweed (1972)
	Sodium nitrate-water	Chen and Manganaro (1974)
Cation exchange resin-Dowex 50X8	K^+-H^+-water	Butts et al. (1973)
	K^+-Na^+-water	Butts et al. (1973)
Cation exchange resin-BioRad AG 50W-X4	Glucose-fructose-water	Chen and Emidio (1975)
Cation (Amberlite IR-45) and Anion (Amberlite IRC-50) exchange resins-mixed bed	Sodium chloride-water	Wilhelm et al. (1966)
		Wilhelm et al. (1968)
		Rolke and Wilhelm (1969)
Duolite C265	Potassium nitrate-water	Grevillot (1980)
Duolite ES861	Phenol-water	Costa et al. (1982)
		Almeida et al. (1982)
		Ramalho et al. (1991)
		Ferreira and Rodrigues (1991)
	Chemical System (gas/solid)	
Activated carbon	Ethane-propane	Jenczewski and Myers (1968)
	Argon-propane	Jenczewski and Myers (1970)
	Propane-propylene	Jenczewski and Myers (1970)
Silica gel	Sulfur dioxide-air	Patrick et al. (1972)

reversed during the upward flow. Heating and cooling of the fluid phase is carried out by the hot (7) and cold (6) heat exchangers. Bubble traps are used to prevent gasing out inside the fixed bed.

Product Receivers

The experimental set-up is an open system with three reservoirs: top, bottom and feed reservoirs. The top reservoir receives product when the solution is pumped through the column in upward flow. The bottom reservoir receives product when the solution is passed through the column in downward flow. From the feed reservoir the solution is passed into the top reservoir, with the pump 18 on. Pressure transducers installed at the bottom of the reservoirs were used to detect when one half cycle ends, i.e., when all the solution contained in a reservoir was transferred, either downward or upward. Since the electric signals from the transducers change with the liquid level in each reservoir, the level change with time allows the calculation of flowrates.

Sampling, Collector and Analytical Devices

Bottom and top products were collected at fixed time intervals by a fraction collector, with pumps 19 and 17 working. The fraction collector 5 is equipped with a controller interface kit that provides the necessary commands to communicate with the micro-computer. The interface between the RS232 computer output and the controller inserted in the equipment is obtained with an RS232 adapter. This adapter converts RS232 signal levels into RS422 levels utilized by the controller. The software was written in Turbo C language and is a routine included in the global control program. All the commands consist of an ASCII string preceded by a line-feed and followed by a carriage-return. The serial computer port is used to send the commands

through the RS232 adapter to the controller. When the controller receives a certain string the fraction collector executes the corresponding command, for example to start the time mode to collect the samples. A double three port fractionation valve is mounted in the top of the fraction collector and is used to direct the solution from the top and bottom reservoirs into the glass tubes rack. The solution is passed either to the fractionation valve or to the drain by using two three-way solenoid valves 13 and 14. The samples were analyzed at 272 nm with a digital UV spectrophotometer.

Automation Section

The whole process is controlled by an IBM PC equipped with the interface DT2805 series board data acquisition system, with the following features: 8 analog inputs, 2 analog outputs and two-8 line digital I/O ports which can be used separately to read or write 8 bits, or simultaneously 16 bits. In addition, it exists the DT707-T screw terminal panel with cold junction compensation circuit, that provides screw terminals for the DT2805 series board's input and output signals. The main operations including data acquisition and digital/analog conversions are as follows: i) readings from the thermocouple signals by using the analog inputs-channels 1 to 5; ii) setting the positions of the solenoid valves, ON or OFF, from the two-8 line digital I/O ports; iii) setting the positions of the peristaltic pumps, ON or OFF, when analog voltage is sent or not from the 2 analog outputs; iv) readings from the pressure transducer signals connected to the analog inputs-channels 6 and 7.

Those operations were programmed with software developed in Turbo C language and also included the PCLAB (real time software package) libraries to manipulate the interface board through operation of specific routine calls. The Turbo C program is structured with different subprograms and each subprogram consists of a set of routines. Some routines allow us to calculate the temperatures from the thermocouple signals, the liquid level from the pressure transducer signal in each reservoir and flowrates, to set the valve and peristaltic positions, to stop the parapump operation when an accident happens, to create screen animation, etc.

Basic Data

As was shown in Part I, a complete mathematical model to describe the recuperative parametric pumping system includes equations for conservation of energy and mass, equilibrium relationships, heat and mass transfer kinetics and initial and boundary conditions. To implement model simulation for a particular system, we need basic information about parameter values included in the model (equilibrium parameters, film mass transfer coefficient, intraparticle diffusivity, axial diffusion, axial and radial thermal conductivities and wall heat transfer coefficient) which can be obtained from laboratory experiments.

Adsorption Equilibrium

Adsorption equilibrium isotherms for the system phenol-water/Duolite ES861 are shown in the Figs. 2a and 2b.

Experimental data were fitted by the Langmuir equation,

$$q^* = \frac{Q_\infty K_L C^*}{1 + K_L C^*} \tag{1}$$

where q^* (kg solute/kg dry resin) and C^* (kg solute/m^3 solution) are concentrations in equilibrium of solute in the adsorbent and liquid phases, respectively.

Batch experiments were carried out equilibrating over 3–4 days a given mass of adsorbent-Duolite ES 861 (a macroporous polystyrene resin crosslinked with divinylbenzene) with a given volume of phenolic solution at 20°C or 60°C. Two different samples from a commercial lot were used to obtain equilibrium isotherms. As shown in Figs. 2a and 2b, the sample 1 has a greater adsorption capacity than the sample 2 at 60°C.

In the concentration range up to 0.1 kg/m^3 (100 ppm) of phenol, the equilibrium data can be fairly represented by a straight line,

$$q^* = K(T)C^* \tag{2}$$

Table 3 shows $K(T)$ values and the parameter b for the system under study. The parameter b was introduced by Pigford (1969) as a measure of the separation potential,

Equilibrium parameters values are summarized in Table 2.

$$b = \frac{a}{1 + \bar{m}} \tag{3}$$

where $\bar{m} = \frac{m(T_1)+m(T_2)}{2}$, the deviation $a = \frac{m(T_1)-m(T_2)}{2}$, with T_1-cold temperature and T_2-hot temperature and $m(T)$ is the capacity parameter defined as $m(T) = \frac{(1-\varepsilon)\rho_{sp}K(T)}{\varepsilon}$.

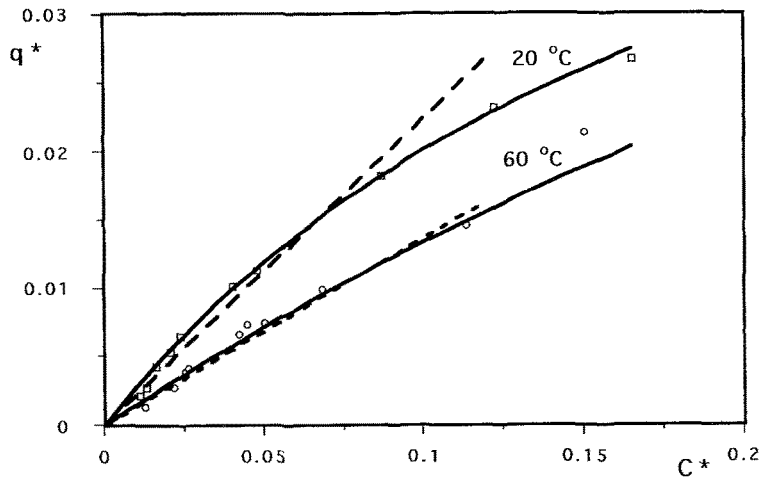

Fig. 2a. Adsorption equilibrium isotherms for phenol on Duolite ES861: □—experimental data at 20°C (sample 1); ○ —experimental data at 60°C (sample 1); — —fitting with Langmuir equation and – – –fitting with linear fitting.

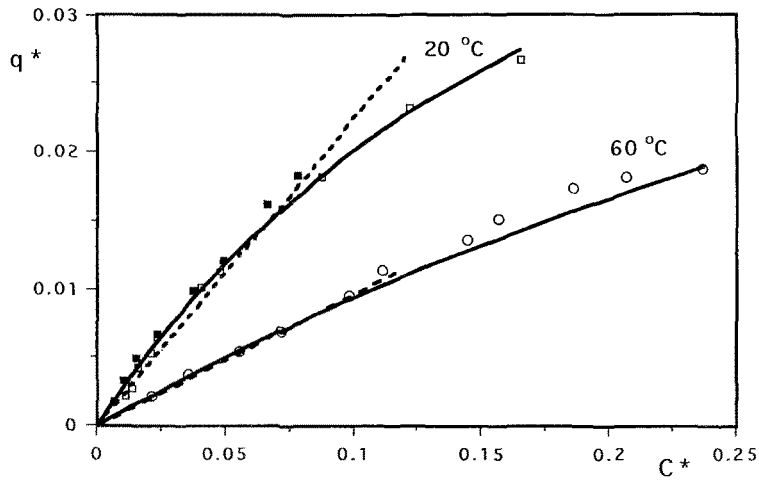

Fig. 2b. Adsorption equilibrium isotherms for phenol on Duolite ES861: □—experimental data at 20°C (sample 1); ■—experimental data at 20°C (sample 2); ○ —experimental data at 60°C (sample 2); — —fitting with Langmuir equation and – – –fitting with linear fitting.

Table 2. Equilibrium parameter values of the Langmuir isotherm.

Sample	Temperature (°C)	K_L (m^3 solution/kg solute)	Q_∞ (10^{-3}) (kg solute/kg dry resin)
1	20	4.60	63.60
1	60	1.45	105.00
2	20	4.60	63.60
2	60	1.45	74.00

As we can see in Table 3, sample 2 presents a larger b parameter value than that of the sample 1; therefore

Table 3. Equilibrium data.

Physical characteristics of the adsorbent Duolite ES861:			
Apparent density ρ_{ap}		285.6 kg/m^3	
Wet density ρ_h		1020 kg/m^3	
Humidity factor f_H (kg dry mass/kg wet mass)		0.28	
Specific surface area SBET		5×10^5 m^2/kg	
System	K (20°C)	K (60°C)	b
Phenol/Duolite ES861 (sample 1)	0.224	0.136	0.20
Phenol/Duolite ES861 (sample 2)	0.224	0.096	0.37

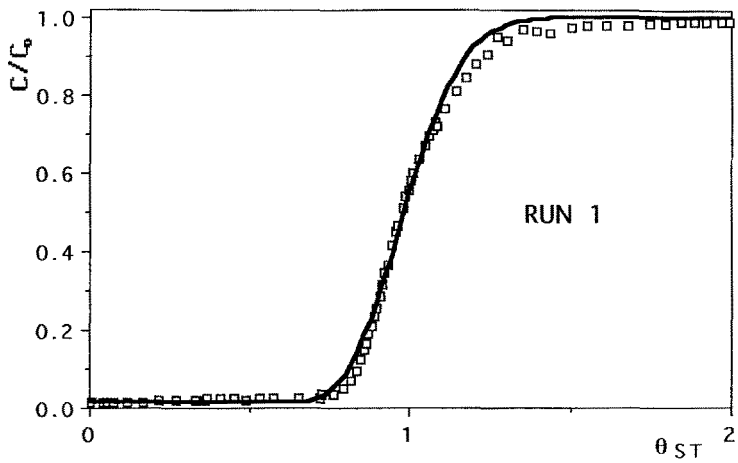

Fig. 3. Breakthrough curve for phenol at 20°C.

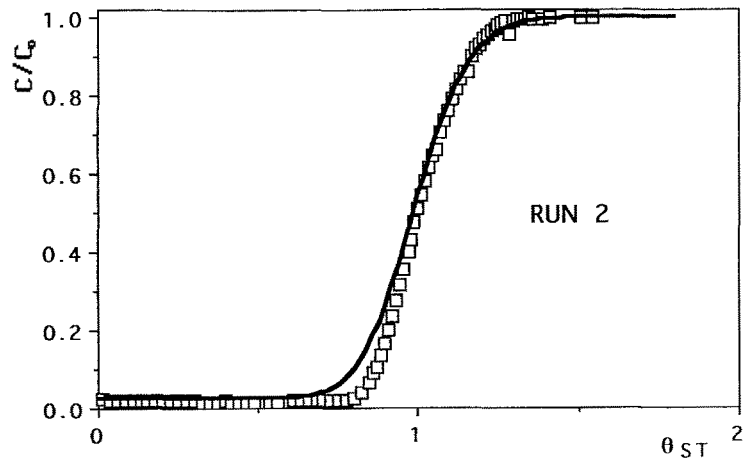

Fig. 4. Breakthrough curve for phenol at 60°C.

better separation in the parametric pumping process would be expected when sample 2 is used.

Mass Transfer

The separation in parametric pumping is limited by dispersive effects of axial dispersion and finite mass transfer rate. In order to evaluate those effects fixed bed experiments were carried out to obtain breakthrough curves, at 20°C and 60°C. Table 4 shows the experimental conditions used. Histories of concentrations are presented in Figs. 3 and 4. Solid lines are simulations with a model that considers axial dispersed plug flow, pore diffusion model and film mass transfer.

The model parameters are:

— adsorption equilibrium parameters K_L and Q_∞
— mass capacity factor $\xi = \frac{(1-\varepsilon)q'_E}{\varepsilon C_E}$ with $q'_E = \varepsilon_p C_E + \frac{K_L Q_\infty C_E \rho_h f_H}{1+K_L C_E}$
— number of film mass transfer units $N_f = \frac{3(1-\varepsilon)k_f \tau}{R_0}$
— number of intraparticle of diffusion units $N_D = \frac{\tau D_P}{R_0^2}$
— Peclet number $\mathrm{Pe} = \frac{uL}{D_{ax}}$.

To evaluate ξ and N_f, the interparticle porosity ε was calculated based on the global mass balance for the column. The values for K_L and Q_∞ were already reported in the equilibrium adsorption study;

Table 4. Experimental conditions for the fixed bed experiments.

Run	T(°C)	Flow direction	q'_E (kg/m^3)	t_{st} (h)	ε	ξ	τ (h)
1	20	Downward	5.755	12.3	0.42	80.0	0.152
2	60	upward	3.836	8.52	0.40	58.0	0.145

Feed flowrate, $Q = 4.28 \times 10^{-6}$ m^3/s; adsorbent capacity at 20°C, $Q_{\infty 1} = 0.0636$ $kg_{solute}/kg_{dry\ resin}$; feed concentration, $C_E = 0.099$ kg/m^3; adsorbent capacity at 60°C, $Q_{\infty 2} = 0.105$ $kg_{solute}/kg_{dry\ resin}$; bed length, $L = 0.87$ m; equilibrium parameter at 20°C, $K_{L1} = 4.6$ $m^3_{solute}/kg_{solution}$; intraparticle porosity, $\varepsilon_p = 0.72$; equilibrium parameter at 60°C, $K_{L2} = 1.45$ $m^3_{solute}/kg_{solution}$; particle diameter, $d_p = 4.7 \times 10^{-4}$ m; wet density of the adsorbent, $\rho_h = 1020$ kg/m^3; humidity factor of the adsorbent, $f_H = 0.28$.

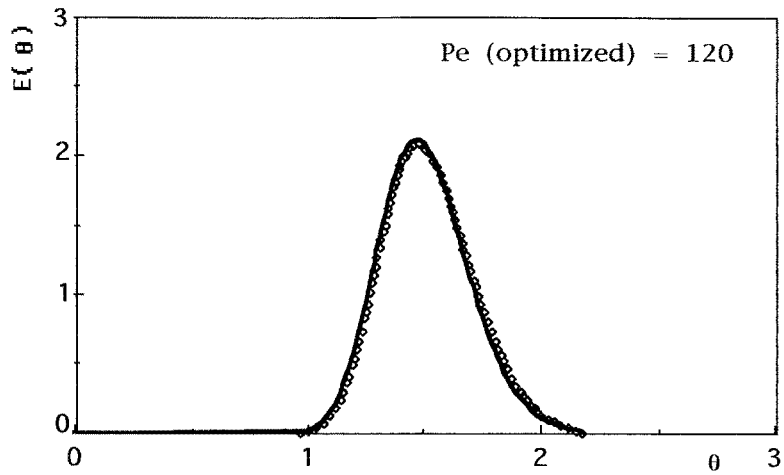

Fig. 5. Experimental (□) and simulated responses (—) of the fixed bed to a tracer injection (experimental conditions: $Q = 4.1 \times 10^{-6}$ m^3/s in downward flow; $L = 0.85$ m; $d = 0.09$ m; $T = 20$°C; $\varepsilon = 0.4$ and $D_{p(tracer)} = 1.67 \times 10^{-9}$ m^2/s, Costa and Rodrigues (1985)).

the film mass transfer coefficient, k_f was determined from j_D-factor correlation, $j_D = 7.32\,Re'^{-0.569}$ (Costa and Rodrigues, 1985) for the system Phenol/Duolite ES861, with $Re' = Re/(1 - \varepsilon)$; Peclet number (Pe) was estimated by analyzing the column hydrodynamics with the concept of residence time distribution (RTD). The information concerning the RTD was obtained using the tracer (KCl) pulse technique. Figure 5 shows one of those experiments. The full lines represent the prediction of a model that considers axial dispersed plug flow and intraparticle diffusion of the tracer. The Peclet number was estimated by multivariable optimization (Rosenbrock method).

The parameter N_D was fitted to the experimental data by using the optimization routine of Rosenbrock and is shown in Table 5. Its value was used to find the tortuosity factor for the adsorbent ($\tau_p = D_m/D_p$ with the molecular diffusivity of phenol in water D_m calculated by Wilke equation, Wilke and Chang (1955)), $\tau_p = 2.93$, in the range 2–6 (Ruthven, 1984) of

Table 5. Model parameters.

T(°C)	N_D	N_f	Pe
20	3.0	700	120
60	7.0	1200	120

experimental tortuosity values generally found for conventional adsorbents.

Phenol effective diffusivities ($\varepsilon_p D_p$, with $\varepsilon_p = 0.72$) at 20°C and 60°C were found to be 2.18×10^{-10} m^2/s and 5.62×10^{-10} m^2/s, respectively.

Heat Transfer

In recuperative mode the entire column does not change the temperature simultaneously, and so we must follow the temperature wave in the column. Since the heat of adsorption is negligible, we can analyze separately the heat transfer process in the column which allows us to

Table 6. Experimental conditions for the thermal experiment.

Flow direction	T_a (°C)	T'_F (°C)	T_{F_0} (°C)	Q (m^3/s)	τ (s)	τ_b (s)	UA (kJ/s.K)
Downward	25	18	60	4×10^{-6}	546	150	5.02×10^{-4}

Bed length $L = 0.85$ m; bed diameter $d = 0.09$ m; interparticle porosity $\varepsilon = 0.4$;
particle diameter $d_p = 4.7 \times 10^{-4}$ m; thermal capacity factor $\xi_h = 1.3$;
density of the adsorbent $\rho_h = 1020$ kg/m^3; density of the fluid $\rho_f^* = 1000$ kg/m^3;
heat capacity of the adsorbent $c_{ps}^* = 1.464$ kJ/kg.k; heat capacity of the fluid $c_{pf}^* = 4.176$ kJ/kg.k.

source:*—Handbook of Chemistry Physics, Weast (1973).

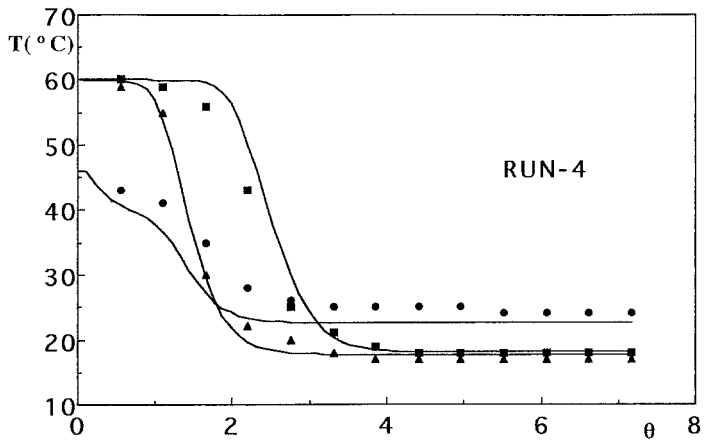

Fig. 6. Histories of experimental and simulated temperatures for Run 4: bottom (■)—$z^* = 0$, $r^* = 0$; middle (△)—$z^* = 0.5$, $r^* = 0$; wall (●)—$z^* = 0.5$, $r^* = 1$.

obtain axial and radial thermal conductivities and the wall heat transfer coefficient.

Experiments to measure thermal parameters start with an initial temperature profile in the column. Then hot or cold feed was pumped through the column at a given flowrate. Temperatures were recorded from thermocouples located at different axial and radial positions in the column. Table 6 shows the experimental conditions of a typical thermal run, in which the average initial temperature was 60°C.

In Table 6, heat capacities (c_{pf} and c_{ps}) were estimated at the average temperature between the cold and hot operating temperatures, 20 and 60°C, respectively.

Figure 6 compares experimental temperature profiles in the fixed bed and results from the simulation with a pseudo-homogeneous two-dimensional model. That model takes into account radial and axial conduction, continuity of heat flux at the wall and considers the adsorbent locally in equilibrium with the fluid and an exponential change in the feed temperature at the bed inlet due to the bubble traps that contain a small volume of solution at uniform temperature.

Model parameters are: $Pe_h^* = G_f c_{pf} d_p / K_{ae}$, $Pe_r^* = G_f c_{pf} d_p / K_{re}$, $\xi_h = (1 - \varepsilon)\, \rho_h c'_{ps} / (\varepsilon \rho_f c_{pf})$ and $Bi = \alpha_w R_c / K_{re}$. The thermal capacity parameter ξ_h was evaluated on the basis of the heat capacity ratio of both phases. The value of 0.72 kg water/kg wet resin (water content of the wet resin) obtained in the equilibrium study was used to calculate c'_{ps} (= 3.42 kJ/kg wet resin.K).

From a fit of the experimental data using model numerical solution we estimate $Pe_h^* = 0.044$, $Pe_r^* = 8.7$ and $Bi = 8.6$. With these parameter values we find, $K_{ae} = 2.773 \times 10^{-2}$ kJ/(m.s.K), $K_{re} = 1.46 \times 10^{-4}$ kJ/(m.s.K) and $\alpha_w = 2.79 \times 10^{-2}$ kJ/(m^2.s.K).

The simulation of the recuperative parametric pumping process is obtained by solving numerically a system of heat and mass transfer (two spatial dimensional model in r and z) differential equations, with the appropriate boundary and initial conditions. Use of a two-dimensional heat transfer model drastically increases the CPU time, since an additional spatial dimension R is involved in the system. We will assume that a

Table 7. Experimental conditions of the parametric pumping runs.

Run	$Q_{hc} \times 10^6$ m^3/s	$Q_{cc} \times 10^6$ m^3/s	$Q_{tp} \times 10^6$ m^3/s	$Q_{bp} \times 10^6$ m^3/s	C_F kg/m^3	t_{hc} min	t_{cc} min	T_h (°C)	T_c (°C)	T_s (°C)
1	4.470	5.130	0.245	0.518	0.098	128	138	60	18	24
2	4.670	5.080	0.200	0.500	0.098	70	86	58	20	21
3	4.170	4.420	0.800	1.080	0.096	88	140	58	18	19
4	4.030	5.130	2.000	1.967	0.098	48	55	60	18	22
5	4.420	3.530	0.830	1.667	0.105	89	152	60	18	24
6	4.667	3.330	1.283	2.567	0.110	55	119	60	18	24
7	4.833	3.667	0.667	1.333	0.096	108	181	60	18	21
8	4.833	4.333	3.117	0.350	0.098	50	60	60	18	25
9	4.833	4.333	2.867	1.433	0.100	54	78	60	18	24
10	2.750	4.000	1.633	0.433	0.104	91	72	60	22	24
11	6.000	4.833	1.633	0.433	0.096	35	50	60	20	25
12	2.500	3.667	1.583	0.417	0.098	118	98	57	22	22

pseudo-homogeneous one-dimensional model (uniform radial temperature) should approximate well the thermal responses to changes in feed temperature at ends of the column. Fitting the experimental data (averaged temperatures in radial direction) at the bottom and middle of the column, using the analytical steady-state solution of the one-dimensional model, we find an average wall heat transfer coefficient $h_w = 1.42 \times 10^{-2}$ kJ/(m^2.s.K).

Using the formula ($1/h_w = 1/\alpha_w + R_c/\beta K_{re}$) derived from the equivalence between the pseudo-homogeneous one-dimensional and two-dimensional mode, Dixon (1985), we obtain $\beta \approx 9$. Various values of β have been used depending on the numerical analysis of the model equations. Villadsen and Michelsen (1978) showed that the best choice leads to $\beta = 4$. To calculate β we used parameters (α_w, K_{re}) that were estimated solving transient solution of the two-dimensional model. This can probably justify the discrepancy between the two β values, knowing that the previous formula is derived from steady state solutions of the one and two-dimensional models.

Simulation of Experimental Parametric Pumping Runs

All experiments of the parametric pumping were carried out by operating the pilot plant shown in Fig. 1. Experimental conditions are summarized in Table 7. Each run was started by equilibrating the adsorbent (Duolite ES861—sample 2) with a solution containing phenol with feed concentration (≈100 ppm) at the hot temperature (≈60°C), except in the run 2 where the adsorbent (sample 1) was equilibrated at the cold temperature (≈20°C).

Feed to the top reservoir and product (top and bottom) withdrawals were performed continuously during each cycle for the runs 1, 2 and 3. In the remaining runs the operation was semi-continuous, i.e., feed input and top product withdrawal during the hot half cycle (upward flow) and bottom product withdrawal during the cold half cycle (downward flow).

In each experiment, transient evolution of the top and bottom products was followed measuring the phenol concentration by UV spectrophotometry at 272 nm.

The runs will be now simulated using the basic information previously determined, related with equilibrium, mass and heat transfer parameters. Equilibrium and complete models developed in Part I will be used to describe the experimental behavior of the parametric pumping process.

Simulation with the Equilibrium Model

Let us analyze the experimental results concerning the runs 1, 2 and 3 with an equilibrium model based on the following assumptions: linear isotherm, no heat transfer resistances (direct mode), no mass transfer resistances, no pressure drop, plug flow for the bulk fluid phase. Chen et al., 1972 developed a model based on these assumptions. According to their results the top and bottom product concentrations can be calculated by:

$$\frac{\langle C_{BP} \rangle_n}{C_0} = \frac{1-b}{1+b}\left[\frac{\frac{1-b}{1+b} + m_2}{1+m_2}\right]^{n-1}, \quad n \geq 1 \qquad (4)$$

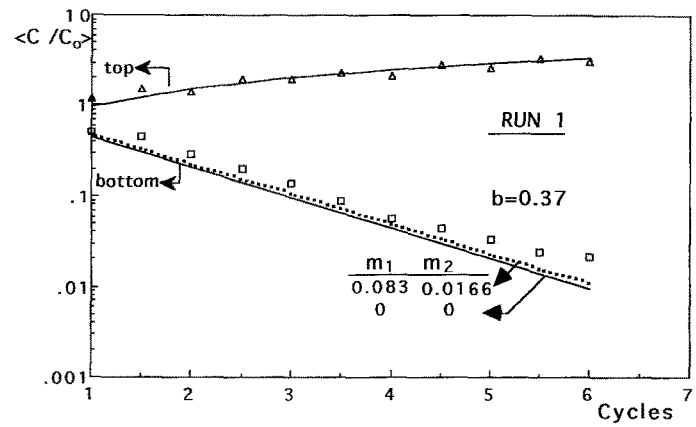

Fig. 7. Top and bottom product concentrations as a function of number of cycles in recuperative mode parametric pumping (Run 1). Comparison between experimental results and equilibrium model ($L = 0.85$ m, $d = 0.09$ m, $\phi_B = 0.10$, $\phi_T = 0.049$, $Q(\pi/\omega) = 0.0382$ m^3, $V_U = 0.0343$ m^3 and $V_D = 0.0425$ m^3).

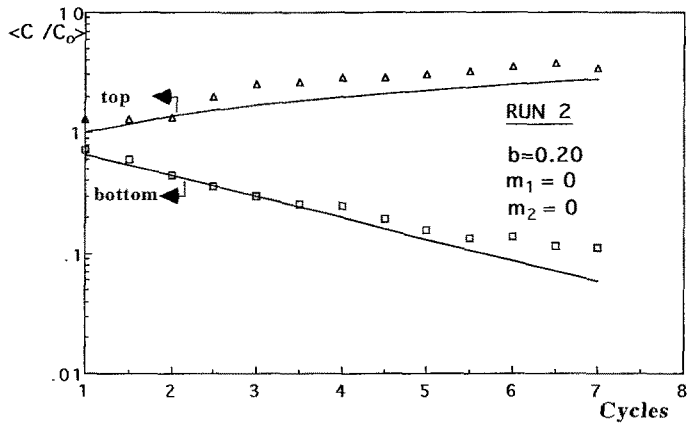

Fig. 8. Top and bottom product concentrations as a function of number of cycles in recuperative mode parametric pumping (Run 2). Comparison between experimental results and equilibrium model ($L = 0.85$ m, $d = 0.09$ m, $\phi_B = 0.10$, $\phi_T = 0.04$, $Q(\pi/\omega) = 0.0224$ m^3, $V_U = 0.0203$m^3 and $V_D = 0.0249$ m^3).

$$\frac{\langle C_{TP}\rangle_n}{C_0} = -\frac{\phi_T+\phi_B}{1-\phi_T} + \frac{1+\phi_B}{1-\phi_T} \times \left[\frac{(1-\phi_T)/(1+\phi_T)+m_1}{1+m_1}\right]^{n-1} + \frac{1+\phi_B}{1-\phi_T}\frac{1+\phi_T}{2\phi_T}\left[1-\frac{1-\phi_T(1-b)}{1+\phi_T(1+b)}\right] \times \left\{1-\left[\frac{(1-\phi_T)/(1+\phi_T)+m_1}{1+m_1}\right]^{n-1}\right\}, \quad n \le p_1+1 \qquad (5)$$

where $p_1+q_1 = \frac{L-L_2}{L_1-L_2}$; p_1 = zero or a positive integer and $0 \le q_1 \le 1$.

Figure 7 shows experimental results for the first run using a cycle time t_c of 4.43 h. After 6 cycles the bottom product concentration was reduced about 0.02 × initial feed concentration. As it can be seen more cycles were needed to know how this concentration should still decrease until the steady state. More cycles were carried out in run 3, as shown in Fig. 9. This run used a cycle time lower ($t_c = 3.8$ h) than the previous one because the hot half cycle time was decreased. We note that a steady state bottom product concentration of about 0.04 × initial feed concentration was observed. Thus, a decrease in the cycle time should yield a less purified bottom product.

Figure 8 represents experimental results for the run 2; the adsorbent (sample 2) used presents a lower b

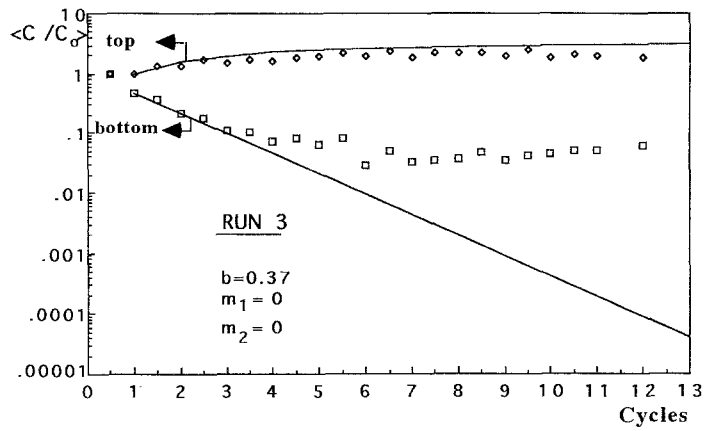

Fig. 9. Top and bottom product concentrations as a function of number of cycles in recuperative mode parametric pumping (Run 3). Comparison between experimental results and equilibrium model ($L = 0.85\,\text{m}$, $d = 0.09\,\text{m}$, $\phi_B = 0.206$, $\phi_T = 0.152$, $Q(\pi/\omega) = 0.02772\,\text{m}^3$, $V_U = 0.0220\,\text{m}^3$ and $V_D = 0.03682\,\text{m}^3$).

Table 8. Parameters values used in simulations with the complete model.

Resin properties	Bed characteristics	Equilibrium data	Thermal parameters	Transport parameters
$\varepsilon_p = 0.72$	$\varepsilon = 0.4$ (upward flow) / 0.42 (downward flow)	$K_L = 3.96 \times 10^{-3} \times \exp(-\Delta H/R_g T)$ (m³/kg)	$\text{Pe}_h = 80$	$\text{Pe} = 120$
$R_0 = 2.35 \times 10^{-4}$ m			$\xi_h = 1.3$	$D_m = 8.9 \times 10^{-10}$ (m²/s) (at 20°C)
$f_H = 0.28$			$\bar{h}_w = 1.42 \times 10^{-2}$ kJ/(m²·s.K)	
$\rho_h = 1020\,\text{kg/m}^3$	$d = 9 \times 10^{-2}$ m	$(-\Delta H/R_g) = 2744$ K		$D_m = 2.2 \times 10^{-9}$ (m²/s) (at 60°C)
$\tau_p = 3$		$Q_\infty = 0.0636\,\text{kg}_{\text{sol}}/\text{kg}_{\text{resin}}$ (at 20°C)		
		$Q_\infty = 0.074\,\text{kg}_{\text{sol}}/\text{kg}_{\text{resin}}$ (at 60°C)		

(separation parameter) value than that of the runs 1 and 3 and so less separation was obtained.

In the three figures experimental and equilibrium model results using Eqs. (4) and (5) are compared. This model gives good predictions for the initial cycles, in which a linear decrease (in semi-log plot) of the bottom product concentration is observed. As dispersive effects become more significant (after 4–5 operating cycles), we notice an increasing deviation of the trend of the experimental bottom product concentration linear. However, model results seem to follow reasonably the trend of the experimental top product concentrations until the steady state.

As shown in Fig. 7, dead volumes are insignificant and do not influence the transient behavior of the product concentrations. In further results these volumes are always neglected.

Simulation with the Complete Model

It is expected that the complete model will give more realistic results than those obtained with the equilibrium model. As shown in Part I (Ferreira and Rodrigues, 1995), the complete model includes mass and heat transfer effects that cause a finite separation. According to this model, the bottom product concentration should approach asymptotically a small value instead of decreasing to zero.

The model solution uses the basic information summarized in Table 8.

Figure 10 shows simulated results of one of the continuous experiments (Run 3) using the complete model. A satisfactory agreement between model and experimental results is obtained.

A comparison of simulated results using equilibrium and complete models, in which the bottom and top

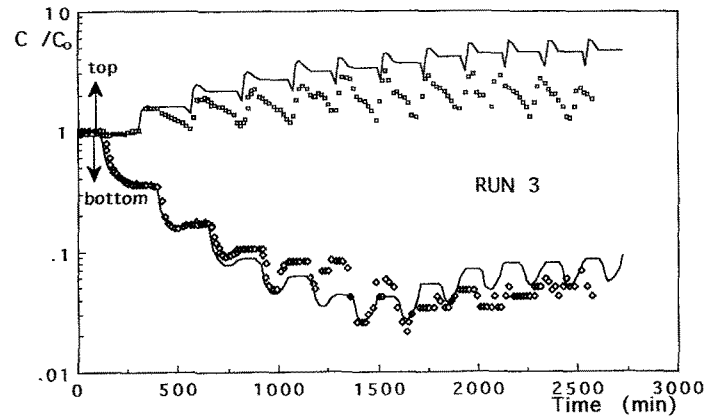

Fig. 10. Top and bottom product concentrations as a function of time in recuperative mode parametric pumping (Run 3). Full lines are simulated results with the complete model.

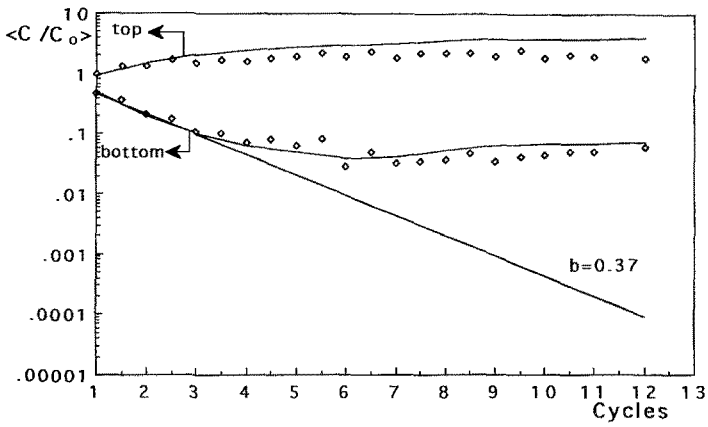

Fig. 11. Top and bottom product concentrations as a function of number of cycles in recuperative mode parametric pumping (Run 3). Full lines are simulated results with the complete and equilibrium ($b = 0.37$) models.

concentrations are averaged in each operating half cycle, is shown in Fig. 11. Analyzing the last two figures, we can observe that the experimental top concentration is over predicted by the complete model, probably because a mixed reservoir volumes was assumed. In the real situation the reservoirs must be considered as partially mixed; in fact the history of concentration in the volumes contained in the reservoirs is defined as boundary conditions for the numerical solution of the model and affects the separation.

The complete model will be used to describe semi-continuous parametric pumping runs. We attempt to explore different operating conditions looking for the best experimental situation to purify the wastewater. It should be pointed here that this does not mean that wastewater purification is an interesting application for parametric pumping; it is just a test example based on a system in which our laboratory had previous experience.

Effect of the Cycle Time. This effect was studied by carrying out runs 5, 6 and 7, by changing the volume percolated in upward flow (hot half cycle) and setting the following conditions:

- Production $(V_B + V_T) = 13\ \ell$)
- Ratio $(V_B/V_T) = 2$
- Average flowrate $= 4.083 \times 10^{-6}$ m^3/s

Figure 12 compares experimental and simulated results using the complete model (full lines) for the run 5. In that figure one can see the behavior of the histories of top and bottom concentrations for a semi-continuous parametric pumping experiment. During

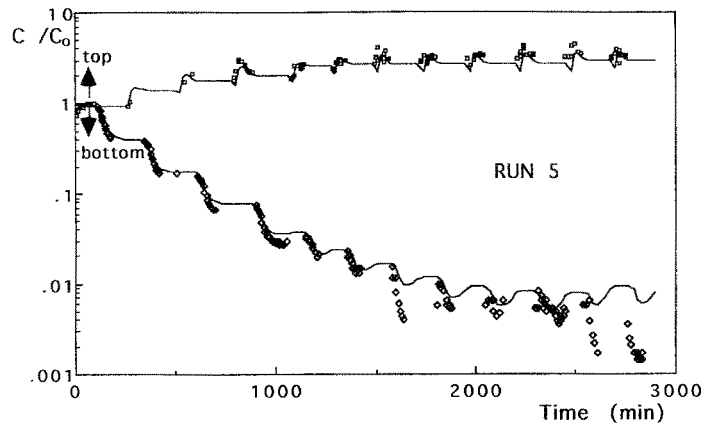

Fig. 12. Top and bottom product concentrations as a function of time in recuperative mode parametric pumping (Run 5). Full lines are simulated results with the complete model ($L = 0.85\,\text{m}$, $d = 0.09\,\text{m}$, $\phi_B = 0.27$, $\phi_T = 0.14$, $Q(\pi/\omega) = 0.0325\,\text{m}^3$, $V_U = 0.02360\,\text{m}^3$ and $V_D = 0.0325\,\text{m}^3$).

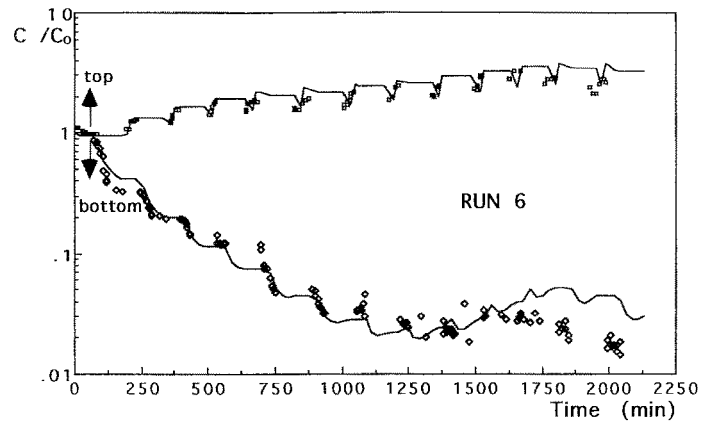

Fig. 13. Top and bottom product concentrations as a function of time in recuperative mode parametric pumping (Run 6). Full lines are simulated results with the complete model ($L = 0.85\,\text{m}$, $d = 0.09\,\text{m}$, $\phi_B = 0.34$, $\phi_T = 0.14$, $Q(\pi/\omega) = 0.0239\,\text{m}^3$, $V_U = 0.0154\,\text{m}^3$ and $V_D = 0.0239\,\text{m}^3$).

the hot half cycle, an increase in the top concentration is observed because the solute inside of the column is desorbed. During the cold half cycle, more solute is adsorbed and as bottom product we collect a solution of decreasing concentration. Figure 12 also shows that some discrepancies between experimental and simulated results occur at the end of the run. This situation may be justified by considering that for the last cycles the solute concentration is very low and higher experimental error can be observed when the samples are analyzed.

Figures 13 and 14 show experimental and model results for the runs 6 and 7. A comparison of results corresponding to runs 5, 6 and 7 can be seen in Fig. 15, where the effect of the cycle time is enhanced. At short cycle times the bottom product concentration tends to stabilize around a higher value and a poor purification of the solvent is obtained. With long cycle times one can expect better results, in terms of the solvent purification, because interphase mass transfer is improved. Figure 15 also shows that better agreement between the experimental and simulated results by the equilibrium model ($b = 0.37$) is obtained for the run 7. This is so because that run was carried out at longer cycle time causing the operation closer to the equilibrium conditions.

Looking now the behavior of the top product concentration, we note that it tends to a very near value to the steady state value calculated by the equation (Chen and Hill, 1971)

$$\frac{\langle C_{TP}\rangle_\infty}{C_0} = 1 + \frac{\phi_B}{\phi_T} \approx 3 \tag{6}$$

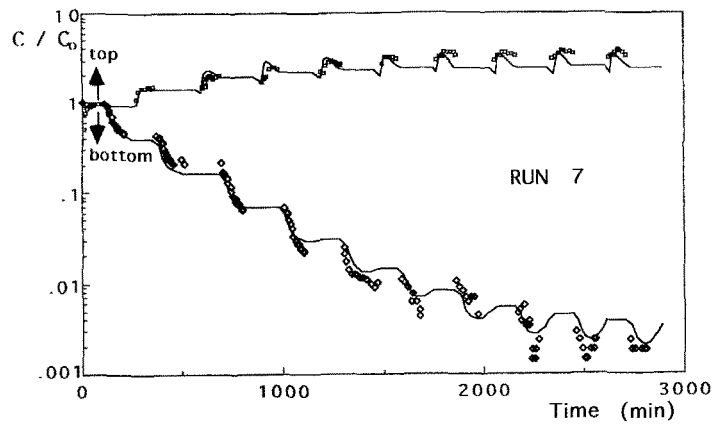

Fig. 14. Top and bottom product concentrations as a function of time in recuperative mode parametric pumping (Run 7). Full lines are simulated results with the complete model ($L = 0.85$ m, $d = 0.09$ m, $\phi_B = 0.22$, $\phi_T = 0.11$, $Q(\pi/\omega) = 0.03996\,\text{m}^3$, $V_U = 0.03132\,\text{m}^3$ and $V_D = 0.03996\,\text{m}^3$).

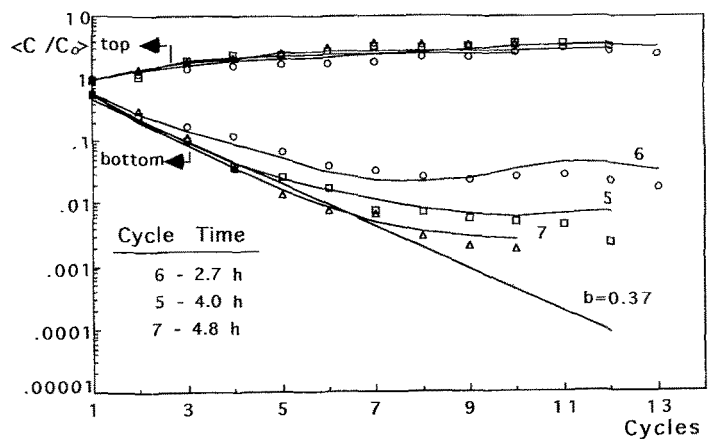

Fig. 15. Top and bottom product concentrations as a function of number of cycles in recuperative mode parametric pumping (Runs 5, 6 and 7). Full lines are simulated results with the equilibrium ($b = 0.37$) and complete models. Effect of the cycle time.

Effect of the Ratio between Fractions of Volume Reservoir Obtained as Bottom and Top Product ϕ_B/ϕ_T. This effect was explored in runs 4, 8 and 9, by changing the ratio ϕ_B/ϕ_T and setting the following conditions:

- $\phi_B + \phi_T = 0.7$
- Average time cycle = 1.87 h

The behavior of the top and bottom product concentrations as a function of the time, for the runs 4, 8 and 9, are represented in Figs. 16, 17 and 18, respectively. A satisfactory agreement between experimental and complete model results (full lines) was obtained.

The effect of the ratio (ϕ_B/ϕ_T) can be seen in Fig. 19, where the results concerning the three experiments are compared. At fixed $(\phi_B + \phi_T)$ and cycle time t_c that ratio has influence on the separation; higher (ϕ_B/ϕ_T) ratios yield a bottom product more concentrated. This result can be understood if we analyze the effect of ϕ_B on the penetration distance L_2 of the concentration wave during the cold half cycle. In fact, when the ratio (ϕ_B/ϕ_T) increases (by increasing ϕ_B) larger top reservoir volume is percolated in downward flow and then L_2 increases. If L_1 (penetration distance during the hot half cycle) is kept constant, larger L_2 leads to little net penetration of the solute $\Delta L = L_1 - L_2$ and less separation is obtained; in this case the bottom concentration reaches a higher steady state value.

Effect of the Flowrate. This effect was explored in runs 10, 11 and 12, by changing the flowrate of the fluid

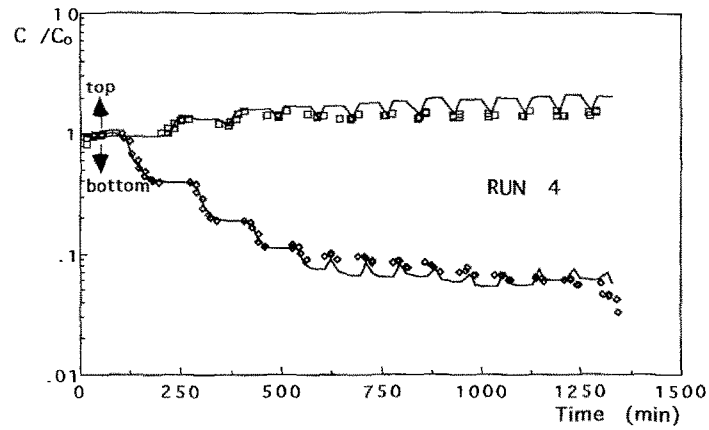

Fig. 16. Top and bottom product concentrations as a function of time in recuperative mode parametric pumping (Run 4). Full lines are simulated results with the complete model ($L = 0.85$ m, $d = 0.09$ m, $\phi_B = 0.31$, $\phi_T = 0.34$, $Q(\pi/\omega) = 0.01695$ m^3, $V_U = 0.01162$ m^3 and $V_D = 0.01695$ m^3).

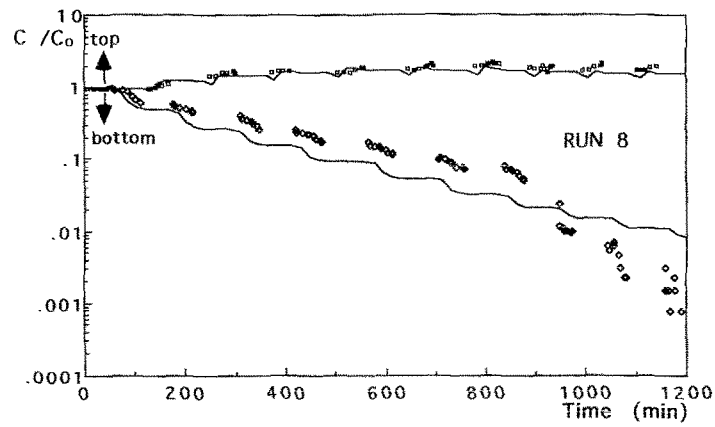

Fig. 17. Top and bottom product concentrations as a function of time in recuperative mode parametric pumping (Run 8). Full lines are simulated results with the complete model ($L = 0.85$ m, $d = 0.09$ m, $\phi_B = 0.068$, $\phi_T = 0.602$, $Q(\pi/\omega) = 0.01555$ m^3, $V_U = 0.0145$ m^3 and $V_D = 0.01555$ m^3).

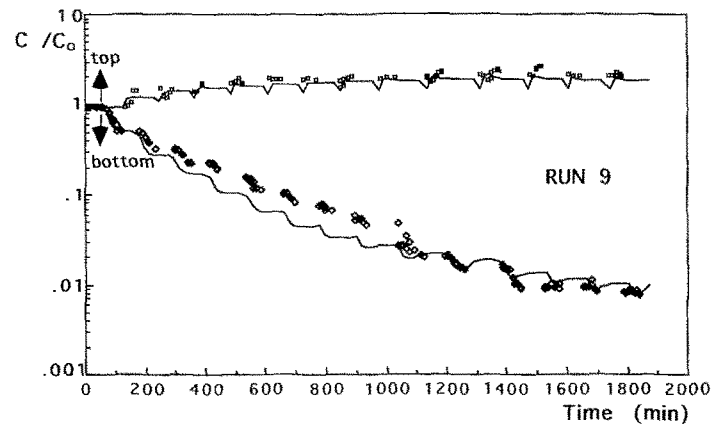

Fig. 18. Top and bottom product concentrations as a function of time in recuperative mode parametric pumping (Run 9). Full lines are simulated results with the complete model ($L = 0.85$ m, $d = 0.09$ m, $\phi_B = 0.23$, $\phi_T = 0.46$, $Q(\pi/\omega) = 0.020304$ m^3, $V_U = 0.01566$ m^3 and $V_D = 0.020304$ m^3).

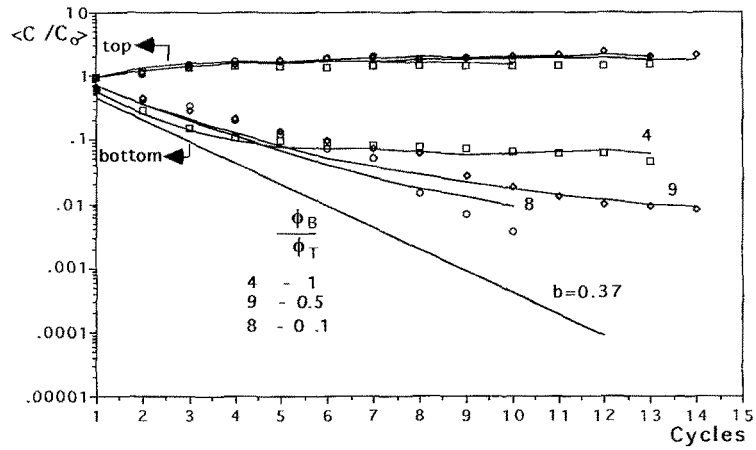

Fig. 19. Top and bottom product concentrations as a function of number of cycles in recuperative mode parametric pumping (Runs 4, 8 and 9). Full lines are simulated results with the equilibrium ($b = 0.37$) and complete models. Effect of the ratio ϕ_B/ϕ_T.

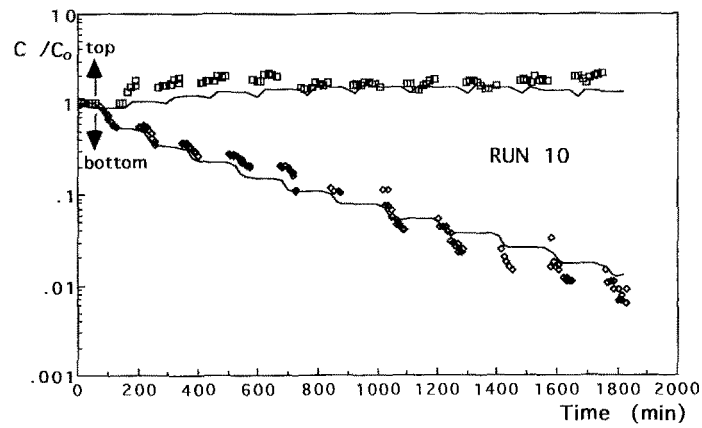

Fig. 20. Top and bottom product concentrations as a function of time in recuperative mode parametric pumping (Run 10). Full lines are simulated results with the complete model ($L = 0.83$ m, $d = 0.09$ m, $\phi_B = 0.14$, $\phi_T = 0.51$, $Q(\pi/\omega) = 0.017381$ m^3, $V_U = 0.015015$ m^{3}and $V_D = 0.017381$ m^3).

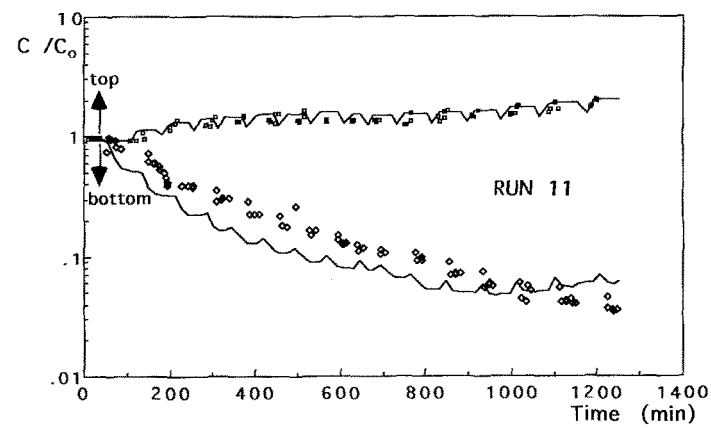

Fig. 21. Top and bottom product concentrations as a function of time in recuperative mode parametric pumping (Run 11). Full lines are simulated results with the complete model ($L = 0.83$ m, $d = 0.09$ m, $\phi_B = 0.13$, $\phi_T = 0.50$, $Q(\pi/\omega) = 0.014252$ m^3, $V_U = 0.0126$ m^3 and $V_D = 0.014525$ m^3).

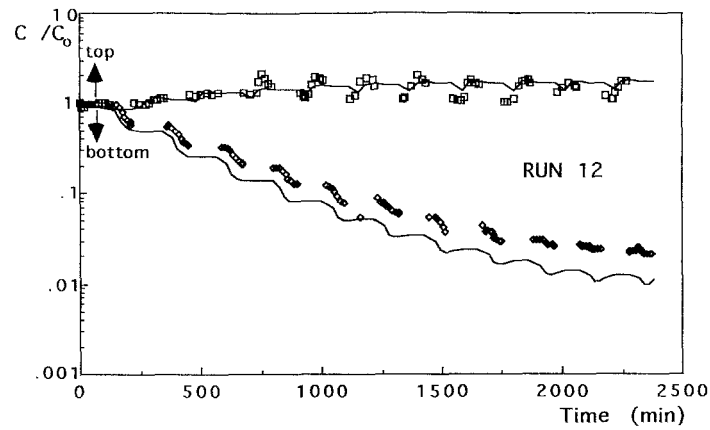

Fig. 22. Top and bottom product concentrations as a function of time in recuperative mode parametric pumping (Run 12). Full lines are simulated results with the complete model ($L = 0.85\,\text{m}$, $d = 0.09\,\text{m}$, $\phi_B = 0.14$, $\phi_T = 0.54$, $Q(\pi/\omega) = 0.020650\,\text{m}^3$ $V_U = 0.0177\,\text{m}^3$ and $V_D = 0.02065\,\text{m}^3$).

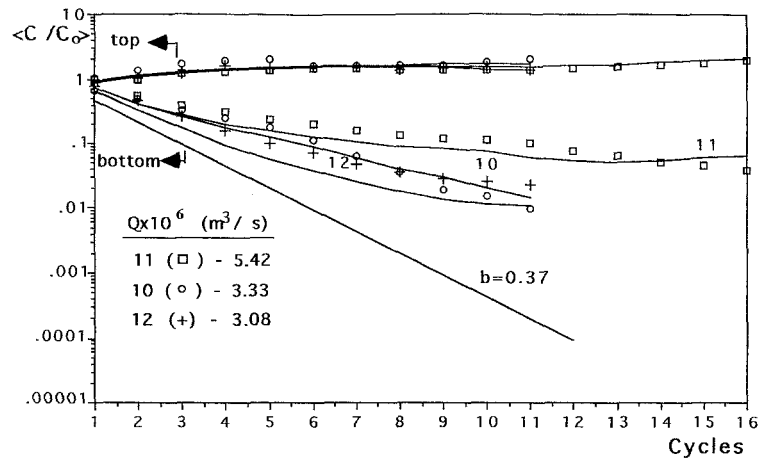

Fig. 23. Top and bottom product concentrations as a function of number of cycles in recuperative mode parametric pumping (Runs 10, 11 and 12). Full lines are simulated results with the equilibrium ($b = 0.37$) and complete models. Effect of the flowrate Q.

in the column either in upward flow or in downward flow (see Table 7) and setting the following conditions:

- $\phi_B + \phi_T = 0.64$
- $\phi_B/\phi_T = 0.27$

In Figs. 20, 21 and 22 we can see the behavior of the top and bottom product concentrations as a function of the time, for the runs 10, 11 and 12, respectively. The complete model results agree satisfactory with the experimental points. Relatively the effect in study, from Fig. 23, we can conclude that best results are obtained operating at low flowrates. This is expected because when the flowrate decreases, i.e., the cycle time increases and a longer contact between the phases is established.

Conclusions

The complete model was used to simulate parametric pumping experiments, on recuperative mode, for several operating conditions. Basic information about equilibrium, mass and heat transfer resistances for the system phenol-water/Duolite ES861 was obtained to determine all model parameters needed for the simulation.

The influence of operating variables (cycle time t_c, the ratio between fractions of volume reservoir obtained as bottom and top product ϕ_B/ϕ_T and flowrate Q) on the solvent purification was studied. Now, we should conclude about optimal conditions to produce a bottom product (aqueous solution) with very small concentration of phenol. Analyzing all the parametric pumping runs done, we have chosen experimental conditions corresponding to Run 5: semi-continuous mode, cycle time = 4 h, $\phi_B/\phi_T = 2(\phi_B = 0.27)$, average flowrate = 4×10^{-6} m^3/s (0.24 ℓ/min) and $Q(\pi/\omega) = 0.0325$ m^3. Based on the productivity of 8.78 ℓ per cycle, 105 ℓ of water almost pure ($C_{\text{phenol}} \leq 1$ ppm) was produced during approximately 2 days of operation. Referring to productivity, we believe that it could be improved by considering the continuous mode, the percolate in the column larger reservoir volumes in each half cycle and to withdraw more solution as bottom product.

This work was directed to the study of scale-up conditions of the parametric pumping for the system phenol-water/Duolite ES861. Using a column diameter six times larger than the laboratory column used in previous work we can conclude that:

- careful packing leads to good hydrodynamics that approaches plug flow;
- the separation is controlled by mass transfer limitations within the range of experimental conditions used;
- the system behaves close to the direct mode of operation; thermal equilibrium is quickly reached and the existence of radial temperature gradients do not influence the separation;
- the pilot plant for recuperative parametric pumping was able to produce clean water;
- the complete model allowed good process simulation and can serve as the basis for the design of para-pumping systems.

Nomenclature

A	heat transfer area, m^2
b	separation parameter
Bi	Biot number ($\alpha_w R_c/K_{\text{re}}$
C	solute concentration in the fluid phase, kg/m^3
c_{pf}	heat capacity of the fluid, kJ/(kg.K)
C_p	solute concentration in the solid phase, kg/m^3
c_{ps}	heat capacity of the adsorbent, kJ/(kg.K)
d	column diameter, m
D_{ax}	axial dispersion coefficient, m^2/s
D_m	molecular diffusion coefficient, m^2/s
D_P	intraparticle diffusion coefficient of phenol, m^2/s
d_p	particle diameter, m
f_H	humidity factor for the adsorbent (kg dry mass/kg wet mass)
G_f	fluid mass flowrate, kg/(m^2.s)
h_w	global wall heat transfer coefficient, kJ/(m^2.s.K)
$(-\Delta H)$	heat of adsorption, kcal/kg
$K(T)$	slope of the linear isotherm, m^3 solution/kg dry resin
K_{ae}	effective axial conductivity, kJ/(m.s.K)
k_f	film mass transfer coefficient, m/s
K_L	parameter of the Langmuir equation, m^3 solution/kg solute
K_{re}	effective radial conductivity, kJ/(m.s.K)
L	bed height, m
L_i	penetration distances ($i = 1$ = upwards; $i = 2$-downwards)
m_1	dimensionless top dead volume ($C_1/Q(\pi/\omega)$, in which C_1 is the top dead volume, m^3)
m_2	dimensionless bottom dead volume ($C_2/Q(\pi/\omega)$, in which C_2 is the bottom dead volume, m^3)
$m(T)$	capacity parameter
n	number of cycles
N_D	number of mass transfer units for pore diffusion
N_f	number of film mass transfer units
Pe	mass Peclet number
Pe_h^*	thermal Peclet number (based on d_p)
Pe_r^*	thermal radial Peclet number (based on d_p)
q	concentration of the solute in the adsorbent, kg solute/kg dry resin
Q	flowrate of the fluid in the column, m^3/s
Q_∞	maximum capacity of the adsorbent, kg solute/kg dry resin
$Q(\pi/\omega)$	reservoir displacement volume, m^3
r	radial coordinate in the particle, m
R	radial coordinate in the column, m
R_c	column radius, m
R_g	ideal gas constant, kcal/(Kg.K)
R_0	particle radius, m
Re	particle Reynolds number
t	times, s
t_{st}	stoichiometric time, s

t_c	cycle time, s
t_{cc}	cold half cycle time, s
t_{hc}	hot half cycle time, s
T	temperature, K
T_a	ambient temperature, K
u	superficial velocity, m/s
U	global heat transfer coefficient in the bubble trap, kJ/(m^2.s.K)
V_B	volume withdrawn as bottom product per cycle, m^3
V_D	volume percolated in downward flow, m^3
V_T	volume withdrawn as top product per cycle, m^3
V_U	volume percolated in upward flow, m^3
z	spatial coordinate, m

Greek letters

α_w	bed-to-wall heat transfer coefficient, kJ/(m^2.s.K)
ε	bed porosity
ε_p	intraparticle porosity
ρ_{ap}	apparent density of the adsorbent, kg/m^3
ρ_f	density of the fluid, kg/m^3
ρ_s	density of the adsorbent, kg/m^3
ρ_h	wet density of the adsorbent, kg/m^3
ω	frequency of temperature change
ϕ_B, ϕ_T	fractions of the $Q\pi/\omega$ that are withdrawn as bottom and top products, respectively
ξ	mass capacity parameter
ξ_h	thermal capacity parameter
τ	spatial time in the column, s
τ_B	spatial time in the bubble trap, s
τ_P	tortuosity factor
π/ω	duration of half cycle, s
θ	reduced time

Subscripts

a	ambient
ae	effective axial
b	bubble trap
B	bottom
cc	cold half cycle
E	entrance
f	fluid
F	feed
hc	hot half cycle
0	initial
p	particle
re	effective radial
ref	reference
s	solid
T	top
tp	top product
bp	bottom product
$\langle\ \rangle$	average value

Acknowledgment

Financial support from Commission of European Communities (Project EV4V-0072-C(TT)) and JNICT is gratefully acknowledged.

References

Almeida, F., C. Costa, A. Rodrigues, and G. Grevillot, "Removal of Phenol From Wastewater by Recuperative Mode Parametric Pumping," in *Physicochemical Methods for Water and Wastewater Treatment*, L. Pawlowski, (Ed.), pp. 169–178 Elsevier Scientific. Publ. Comp. Amsterdam, 1982.

Bolto, B.A., "Sirotherm Desalination-Ion Exchange with a Twist," *Chem. Tech.*, 303–307 (1975).

Butts, T.J., N.H. Sweed and A.A. Camero, "Batch Fractionation of Ionic Mixtures by Parametric Pumping," *Ind. Eng. Chem. Fund.*, **12**, 467–472 (1973).

Chen, H.T. and F.B. Hill, "Characteristics of Batch, Semicontinuous and Continuous Equilibrium Parametric Pumps," *Sep. Science*, **6**, 411–434 (1971).

Chen, H.T., J.L. Rak, J.D. Stokes, and F.B. Hill, "Separation Continuous Parametric Pumping," *AIChE J.*, **18**, 21, 356–361 (1972).

Chen, H.T., J. Reiss, J.J. Stokes, and F. Hill, "Separation Via Semicontinuous Parametric Pumping," *AIChE J.*, **19**, 31, 589–595 (1973).

Chen, H.T., W. Lin, J. Stokes, and W. Fabisiak, "Separations of Multicomponent Mixtures Via Thermal Parametric Pumping," *AIChE J.*, **20**, 306 (1974).

Chen, H.T. and D'Emidio, "Separations of Isomers Via Thermal Parametric Pumping," *AIChE J.*, **21**, 813–815 (1975).

Chen, H.T. and J.A. Manganaro, "Optimal Performance Of Equilibrium Parametric Pumps," *AIChE J.*, **20**, 1020–1022 (1974).

Costa, C., A. Rodrigues, G. Grevillot and D. Tondeur, "Purification of Phenolic Wastewater by Parametric Pumping: Non Mixed Dead Volume Equilibrium Model," *AIChE J.*, **28**, 1, 73–85 (1982).

Costa, C. and A. Rodrigues, "Design of Cyclic Fixed Bed Adsorption Processes. Part I: Phenol Adsorption on Polymeric Adsorbents," *AIChE J.*, **3**, 1, 1645–1654 (1985).

Dixon, A.G., "Thermal Resistance Models of Packed-Bed Effective Heat Transfer Parameters," *AIChE J.*, **31**, 5, 826–834 (1985).

Ferreira, L.M. and A. Rodrigues, "Scale-up of Adsorptive Parametric Pumping," AIChE Meeting, Los Angeles, 1991.

Ferreira, L.M. and A. Rodrigues, "Adsorptive Separation by Thermal Parametric Pumping, Part I: Modeling and Simulation," *Adsorption J.* (1995).

Gregory, R.A. and N.H. Sweed, "Parametric Pumping: Behavior of Open Systems—Part II. Experiment and Computation," *Chem. Eng. J.*, **4**, 139–148 (1972).

Grevillot, G., "Equilibrium Stages Parametric Pumping Part III. Open Systems at Steady-State-McCabe-Thiele Diagrams," *AIChE J.*, **26**, 120–131 (1980).

Jenczewski, T.J. and A.L. Myers, "Parametric Pumping Separates Gas Phase Mixtures," *AIChE J.*, **14**, 509 (1968).

Jenczewski, T.J. and A.L. Myers, "Separation of Gas Mixtures by Pulsed Adsorption," *Ind. Eng. Chem. Fundam.*, **9**, 216–221 (1970).

Patrick, R.R., J.T. Schrodt, and R.I. Kermode, "Thermal Parametric Pumping of Air-SO_2," *Separat. Sci.*, **7**, 331 (1972).

Pigford, R., B. Baker and D. Blun, "An Equilibrium Theory of the Parametric Pump," *Ind. Eng. Chem. Fund.*, **8**, 144–149 (1969).

Ramalho, E., C. Costa, and A. Rodrigues, "Adsorptive Parametric Pumping for the Purification of Phenolic Effluents," *Separat. Technology*, **1**, 99–107 (1991).

Rolke, R.W. and R.H. Wilhelm, "Recuperative Parametric Pumping. Model Development and Experimental Evaluation," *Ind. Eng. Chem. Fund.*, **8**, 2, 235–246 (1969).

Rice, R.G. and M. Mackenzie, "A Curious Anomaly in Parametric Pumping," *Ind. Eng. Chem. Fund.*, **12**, 486–487 (1973).

Ruthven, D.M., "Principles of Adsorption and Adsorption Processes," I. Wiley, 1984.

Sweed, N.H. and R.A. Gregory, "Parametric Pumping: Modeling Direct Thermal Separations of Sodium Chloride-Water in Open and Closed Systems," *AIChE J.*, **17**, 171–176 (1971).

Sweed, N.H. "Parametric Pumping," in *Progress in Separation and Purification*, E.S. Perry and C.J. Van Oss (Eds.), pp. 171–240, Wiley-Interscience, NY, 1971.

Villadsen, J. and M.L. Michelsen, "Solution of Differential Equation Models by Polynomial Approximation," Prentice-Hall Inc., USA, 1978.

Wilke, C.R. and P. Chang, "Correction of Diffusion Coefficients in Dilute Solutions," *AIChE J.*, **1**, 264–270 (1955).

Wilhelm, R.H., A.W. Rice, and A.R. Bendelius, "Parametric Pumping: A Dynamic Principle for Separation Fluid Mixtures," *Ind. Eng. Chem. Fund.*, **5**, 141–144 (1966).

Wilhelm, R.H., A.W. Rice, R.W. Rolke, and N.H. Sweed, "A Dynamic Principle for Separation Fluid Mixtures," *Ind. Eng. Chem Fund*, **7**, 337–348 (1968).